H842 Journal of The Electrochemical Society, **157** (8) H842-H846 (2010)
0013-4651/2010/157(8)/H842/5/$28.00 © The Electrochemical Society

Interfacial Resistive Properties of Nickel Silicide Thin Films to Doped Silicon

Madhu Bhaskaran, Sharath Sriram,[z] and Anthony S. Holland

Microelectronics and Materials Technology Centre and Platform Technologies Research Institute, School of Electrical and Computer Engineering, RMIT University, Melbourne, Victoria 3001, Australia

Improved means of electrical access to nanotechnology devices and accurate nanoscale characterization of electrical properties of ultrathin layers constituting such electrical contacts is of utmost interest to nanoelectronics researchers. This paper reports on the characterization of interfacial resistive properties of ohmic contacts to doped silicon, incorporating thin films of nickel silicide. Silicon doping was achieved by carefully designed ion implantation of antimony (for n-type) and boron (for p-type). Cross Kelvin resistor test structures were used to extract the specific contact resistivity (SCR) values for the different ohmic contacts fabricated. SCR values, which are quantitative characteristics of interfacial resistive properties, as low as $5.0 \times 10^{-9}\ \Omega\ cm^2$ for contacts to antimony-doped silicon and $3.5 \times 10^{-9}\ \Omega\ cm^2$ to boron-doped silicon were estimated. These experimental results, representing the lowest such values measured, were based on a rigorous evaluation technique and verified by finite element modeling.
© 2010 The Electrochemical Society. [DOI: 10.1149/1.3454214] All rights reserved.

Manuscript submitted March 8, 2010; revised manuscript received May 4, 2010. Published June 25, 2010.

Electrical contacts to devices that pose a low resistance continue to be of interest as the dimensions of devices decrease[1] and nanotechnology demands a better means of creating electrical access.[2] In the semiconductor industry, nickel silicide (NiSi) is being used in present processes for local interconnects and in ohmic contacts.[1] The desire to improve the performance of ohmic contacts creates the need for techniques to better characterize and quantify the performance of such contacts. Specific contact resistivity (SCR) is a quantitative measure of the resistance posed by an interface and is denoted as ρ_c (in $\Omega\ cm^2$).[3]

Multiple techniques have been utilized in measuring SCR values. Test structures based on the transmission line model (TLM) are also commonly used to determine SCR. The limitations of the TLM in measuring low values of SCR (below $1 \times 10^{-7}\ \Omega\ cm^2$) are discussed in Ref. 4. Cross Kelvin resistor (CKR) test structures are suitable for the measurement of low values of SCR, but the use of cumbersome error correction curves to estimate the value of SCR and inherent inaccuracies in the technique served as deterrents for the widespread use of this estimation technique.[5-8]

Recent publications demonstrate techniques for significant improvements in the measurement and extraction of low values of SCR,[9-12] enabling the study of new material combinations. Although these recently reported approaches use both TLM and CKR test structures,[9-12] they all aim to measure low values of SCR. Considering the use of nickel silicide in semiconductor (complementary metal oxide semiconductor) technology to enable low contact resistance, the accurate characterization of contacts incorporating nickel silicide with the identification of doping parameters that tend to decrease SCR values is desirable. These approaches are readily transferable to nanotechnology contacts and their characterization. The motivation of these approaches is to accurately estimate the interfacial resistive properties of the interface in an area-independent manner. This enables the estimation of resistance of nanoscale contacts based on the fabrication and extrapolation of data from micrometer-scale contacts without necessarily fabricating nanoscale contacts.

This paper reports on the characterization of ohmic contacts comprising aluminum to nickel silicide to doped silicon. Here, the aluminum silicide SCR for the conductor–conductor combination is very low,[9] with the silicide–silicon SCR dominating the final result. Silicon was doped with antimony using two implant energy levels to attain two different peak concentrations at the silicide–silicon interface. This paper highlights the influence of the variation in dopant concentration on SCR values and compares these results to SCR values measured for p-type boron implantation. SCR measurements were carried out using CKR test structures (Fig. 1) applying the technique described in Ref. 9 and 12, enabling the accurate extraction of low SCR values. These results are supported by finite element models corresponding to the experimental devices.

Experimental

Ion implantation.— Silicon wafers were rinsed with acetone and isopropyl alcohol and dried using nitrogen. The chosen silicon wafers were of (100) orientation with a resistivity of 1–10 Ω cm. n-Type wafers were used for boron implantation, whereas p-type wafers were used for antimony implantation. The wafers were subject to Piranha cleaning (H_2SO_4:H_2O_2:H_2O::2:1:1 for 15 min) and dipped in buffered hydrofluoric acid (BHF, for 30 s) to remove contamination and native oxide. Oxidation of the wafers was carried out at 1050°C. Dry oxidation was carried out for 10 min, followed by wet oxidation for 5 h, which was followed by dry oxidation for 10 min. The oxygen flow rate was 1 L/min throughout the process. The resulting oxide was ~1.2 μm thick. The thermal SiO_2 on the wafers was patterned (by a BHF etch) to create lower CKR "L's" of varying widths (w) for ion implantation. The CKR arm widths used were 10, 20, and 30 μm. A thin oxide layer of 5–7 nm was grown thermally (dry oxidation, 1050°C, 4 min) to reduce channeling during ion implantation due to the availability of only substrate normal (0°) implantation.

Ion implantation was carried out using a metal vapor vacuum arc (MEVVA) ion source. Antimony (Sb) was used to create n-type

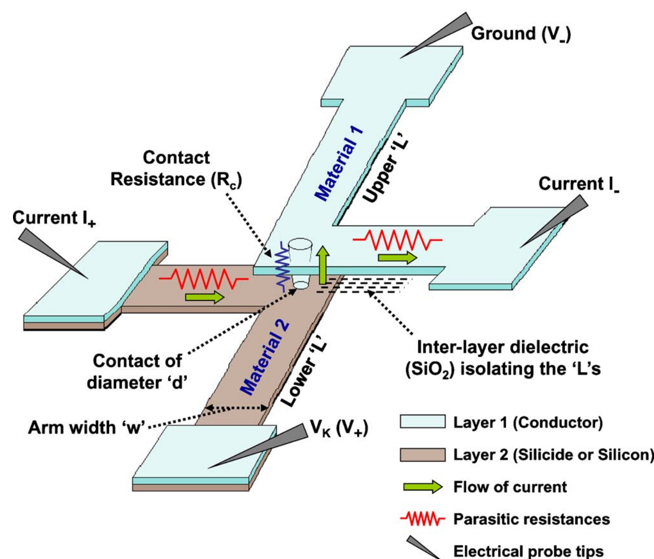

Figure 1. (Color online) Schematic representation of a CKR test structure. Some notations used in this paper are indicated.

[z] E-mail: sharath.sriram@gmail.com

Downloaded on 2016-10-06 to IP 130.203.136.75 address. Redistribution subject to ECS terms of use (see ecsdl.org/site/terms_use) unless CC License in place (see abstract).

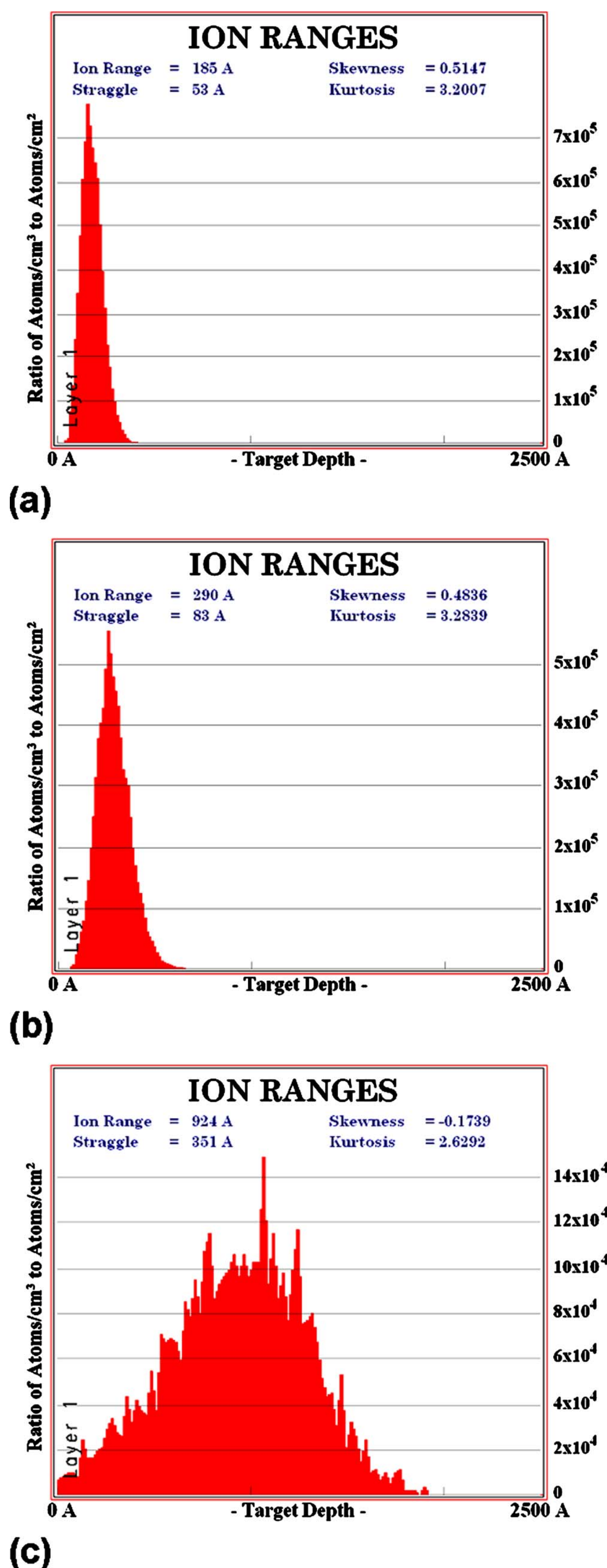

Figure 2. (Color online) Ion range calculations generated using TRIM for implantation of (a) antimony at 20 keV, (b) antimony at 40 keV, and (c) boron at 23.5 keV. All implantations were simulated for an angle of incidence of 0° (substrate normal) related to the capabilities of the MEVVA instrument.

regions, whereas boron (B) was used to define p-type regions. In antimony, the peak concentration was designed to be on or around the NiSi–Si interface depth, resulting from 15 nm of nickel used in the silicidation process. This depth was calculated to be 29 nm.[13-15] In boron doping, the same peak concentration depths could not be replicated as very low implant energies are required (and this was not within the ion implanter capabilities). The energy was chosen to provide a peak dopant concentration at a depth corresponding to the NiSi–Si interface depth (calculated to be 92 nm) resulting from 50 nm of nickel.[13-15] The ion implantation calculations were performed using the popular Stopping Range of Ions in Matter (SRIM) package, 2006 version.[16,17] The TRansport of Ions in Matter (TRIM) calculation function in this package was used to determine appropriate implant energies for antimony and boron to achieve the desired peak concentration depths. The results from TRIM calculations are illustrated in Fig. 2. From these results, the implantation conditions were determined, as summarized in Table I.

Based on these TRIM calculations (Table I), antimony implants at energies of 20 and 40 keV were carried out to create n-type regions in p-type silicon. Likewise, ion implantation of boron was carried out at 23.5 keV to define p-type regions in n-type silicon. A fixed dose of 5×10^{15} atoms/cm^2 was maintained for all implants. After ion implantation, dopant activation was performed by rapid thermal annealing at 1000°C for 40 s in nitrogen ambient.

Fabrication of CKR test structures.— After ion implantation and postimplant anneal, the thermal oxide on the samples was stripped using BHF. The samples were then prepared for lift-off using photolithography (to form circular contacts of different diameters d) following which 100 nm silicon dioxide (SiO_2) was evaporated using electron-beam evaporation at room temperature. Lift-off was completed in an acetone bath. Samples were then coated with 15 nm nickel (50 nm in boron-implanted samples) using electron-beam evaporation. The samples were then vacuum-annealed at 350°C for 10 min (30 min for boron-implanted samples) to form NiSi. Further details of the formation conditions of NiSi are described in Ref. 15. After this self-aligned silicidation step, the unreacted nickel was removed using a 2:1 solution of sulfuric acid and hydrogen peroxide. A 600 nm thick aluminum (Al) layer, deposited by electron-beam evaporation, was patterned to form the upper arms of the CKR test structures. Mask patterns used to define CKR test structures and a plan view of one such fabricated test structure are shown in Fig. 3. The optical micrograph depicting the fabricated test structure (Fig. 2b) was obtained from a sample with antimony implanted at 40 keV, before annealing at 300°C. The cross section of the resulting contact region fabricated is depicted in the schematic in Fig. 4.

Thermal treatment of CKR test structures.— CKR test structures of varying contact sizes (d) and different CKR arm widths (w) were fabricated. The minimum value of diameters of the circular contacts was 0.8–1.0 μm. The maximum contact diameters (d) were chosen based on the CKR arm width (w), such that d/w values of up to ~0.5 were fabricated. For example, for 20 μm width, contacts from 1–10 μm in steps of ~0.5 μm were fabricated.

These Al/NiSi/doped Si contacts were annealed in an atmosphere of 3% hydrogen in nitrogen at 300°C in steps of 30 min to convert them from Schottky to ohmic contacts. SCR measurements of numerous CKR test structures were carried out using a micromanipulator probe station (The Micromanipulator Co.) after each annealing step to study their variations with annealing time (up to 90 min).

Results and Discussion

SCR measurements of Al/NiSi/Sb-doped Si.— Measured SCR values are influenced by parasitic resistance of the surrounding material, which are influence by the CKR geometry (contact diameter d and CKR arm width w). As shown in our previous work, the measured SCR can be analyzed as a function of the ratio d/w.[9,12] Measurements were carried out for many devices with d/w varying from

Downloaded on 2016-10-06 to IP 130.203.136.75 address. Redistribution subject to ECS terms of use (see ecsdl.org/site/terms_use) unless CC License in place (see abstract).

Table I. Ion implantation calculations showing the peak concentration depth. A constant dose of 5×10^{15} atoms/cm^2 was used for all samples.

Implant species	Accelerating voltage (keV)	Ion range R_P (nm)	Ratio of atoms/cm^3 to atoms/cm^2 at R_P
Sb	40.0	29.0	5.60×10^5
Sb	20.0	18.5	8.00×10^5
B	23.5	92.0	1.50×10^5

~0.1 to ~0.5 (for fixed values of w). Tables II and III list the highest and lowest measured SCR values (ρ'_c) for Al/NiSi/Sb-doped Si contacts after different durations of annealing at 300°C. The tables show the maximum and minimum SCR values measured ($\rho'_{c(max)}$ and $\rho'_{c(min)}$, respectively). As the numerical data reach minima ($\rho'_{c(min)}$) as $d/w \to 0$ and maxima ($\rho'_{c(max)}$) near d/w of ~0.5, these values are presented in the tables to provide an indication of the degree of parasitic resistance contributions. These measured values (ρ'_c) include parasitic resistance contribution, and the true SCR value (ρ_c) is extracted from a collection of these values (illustratively described later and as shown in Ref. 9 and 12). The data in Tables II and III demonstrate the effect of annealing, with the best measured SCR results obtained after 90 min of annealing. Further annealing does not impact SCR measurements. SIMS depth profiles were obtained for the entire stack of layers (Al/NiSi/Sb-doped Si) to study the uniformity of layers, verifying that aluminum spiking due to annealing had not occurred, and the positions and relative peak concentrations of the implant species with respect to the NiSi–Si interface. It was observed from the two secondary-ion mass spectrometry (SIMS) depth profiles that the counts corresponding to the concentration of antimony in the samples implanted at 20 keV is ~100 times higher relative to that for the samples implanted at 40 keV. Quantified concentrations could not be obtained due to the unavailability of relevant SIMS standards. The higher concentration in the lower energy implant is along the expected lines (as shown in Table I) as the implant dose in both samples was the same, restricting the dopant to a tighter distribution.

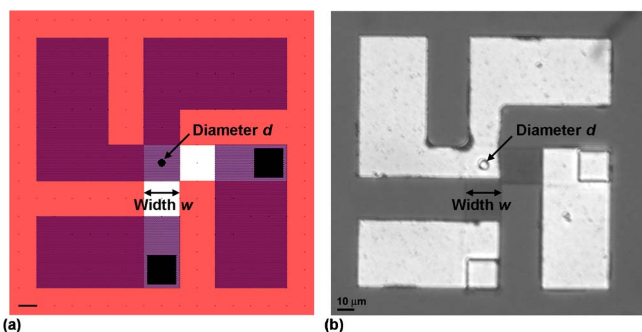

Figure 3. (Color online) (a) An overlaid representation of the three-layer mask patterns used to create lower "L" with w of 20 µm, contact with d of 4 µm, and upper "L" with w of 20 µm of a CKR test structure. (b) An optical micrograph of the fabricated Al/NiSi/Sb-doped Si ohmic contact CKR test structure. The colored regions in (a) represent chromium with the scale bar corresponding to 10 µm.

Table II. Measured and estimated values of SCR for Al/NiSi/Sb-doped Si (implantation energy of 20 keV) ohmic contacts annealed at 300°C for different annealing durations (CKR arm width of 20 µm).

Anneal time (min)	$\rho'_{c(max)}$ (Ω cm^2)	$\rho'_{c(min)}$ (Ω cm^2)	ρ_c (Ω cm^2)
0	1.1×10^{-4}	2.9×10^{-7}	$1.0 \pm 0.5 \times 10^{-7}$
30	3.0×10^{-5}	2.8×10^{-8}	$1.0 \pm 0.5 \times 10^{-8}$
60	5.4×10^{-6}	7.9×10^{-9}	$5.0 \pm 1.0 \times 10^{-9}$
90	5.4×10^{-6}	7.9×10^{-9}	$5.0 \pm 1.0 \times 10^{-9}$

Figure 5 illustrates SCR values measured for the samples implanted with antimony at 40 keV, after 90 min of annealing, for different CKR arm widths w of 8, 10, and 20 µm. Apparently, the measured values of SCR are higher as the CKR arm width increases. This is due to parasitic resistances contributed by the sheet resistance of the two L's, especially the doped silicon region, which increases as w increases.[12] The SCR values determined by extrapolation are between 0.7×10^{-7} and 1.5×10^{-7} Ω cm^2 for the different values of w, which is within acceptable levels of errors in SCR measurements.

A comparison of measured SCR values (for w of 20 µm) after 90 min of annealing for the samples with the two different antimony implant energies is shown in Fig. 6. This figure shows that the SCR of the samples with the higher dopant concentration is much lower. The SCR value for the samples implanted at 20 keV is 5.0 $\times 10^{-9}$ Ω cm^2 vs 1.0×10^{-7} Ω cm^2 for the samples implanted at 40 keV. This significant decrease in SCR can be directly attributed to the ~100 times higher dopant concentration in the 20 keV samples.

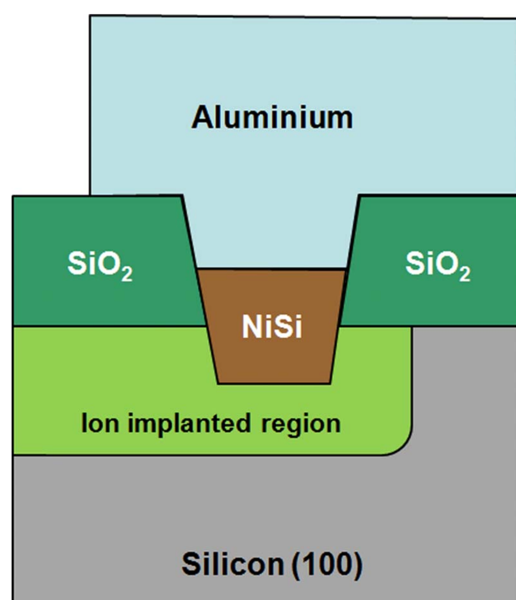

Figure 4. (Color online) Cross-sectional schematic of the fabricated multilayer contact CKR test structure. The aluminum and the ion implanted region form the two "L's." The choice of thicknesses ensured that the Al–NiSi interface lay below the SiO_2 surface, thereby ensuring the isolation between the two "L's" in the CKR test structure (not to scale).

Table III. Measured and estimated values of SCR for Al/NiSi/Sb-doped Si (implantation energy of 40 keV) ohmic contacts annealed at 300°C for different annealing durations (CKR arm width of 20 µm).

Anneal time (min)	$\rho'_{c(max)}$ (Ω cm^2)	$\rho'_{c(min)}$ (Ω cm^2)	ρ_c (Ω cm^2)
0	1.4×10^{-4}	1.8×10^{-6}	$9.0 \pm 1.0 \times 10^{-7}$
30	3.6×10^{-5}	4.6×10^{-7}	$3.0 \pm 0.5 \times 10^{-7}$
60	3.3×10^{-5}	4.0×10^{-7}	$1.0 \pm 0.5 \times 10^{-7}$
90	3.3×10^{-5}	4.0×10^{-7}	$1.0 \pm 0.5 \times 10^{-7}$

Downloaded on 2016-10-06 to IP 130.203.136.75 address. Redistribution subject to ECS terms of use (see ecsdl.org/site/terms_use) unless CC License in place (see abstract).

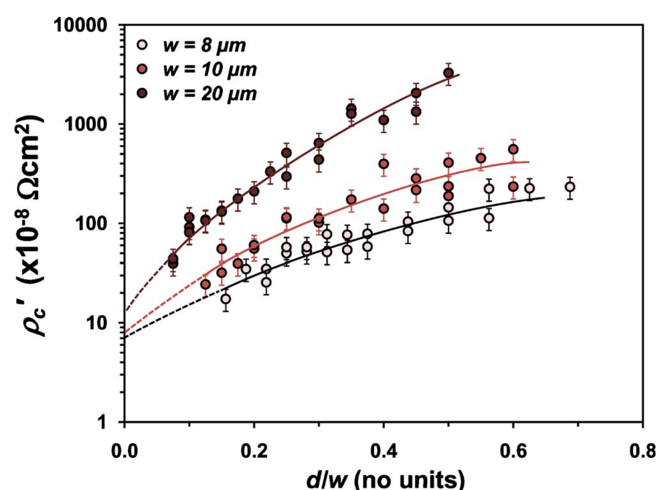

Figure 5. (Color online) Comparison of measured SCR values after 90 min of annealing at 300°C for CKR test structures with silicide arm widths of 8, 10, and 20 μm. These curves were obtained by annealing the sample with antimony implanted at 40 keV. The lines of least-squares fit for each set of data points are shown and the dotted lines are only to assist the reader in extrapolation of the data.

The evaluated SCR value of 5.0×10^{-9} Ω cm^2 is one of the lowest evaluated values reported for a doping concentration of 4.0×10^{21} atoms/cm^3 for an Al/NiSi/Sb-doped Si three-layer contact. The magnitude of this SCR value is comparable to 6.3×10^{-9} Ω cm^2, published in Ref. 10, for a doping concentration of 1.46×10^{20} atoms/cm^3 for a NiSi/As-doped silicon contact.

SCR measurements of Al/NiSi/B-doped Si.— For comparison, similar SCR measurements were also carried out for boron-doped (p-type) silicon. Table IV lists the measured and evaluated values of SCR, with 90 min of annealing yielding an extrapolated ρ_c of 3.5×10^{-9} Ω cm^2. Figure 7 plots measured SCR values before, after 30 min, and after 90 min annealing. The SCR values were obtained for CKR linewidths of 20 μm. There is a significant decrease in SCR values after the first 30 min of annealing, with further annealing causing small changes. The SCR values obtained after 60 and 90 min of annealing were very similar, with further annealing causing

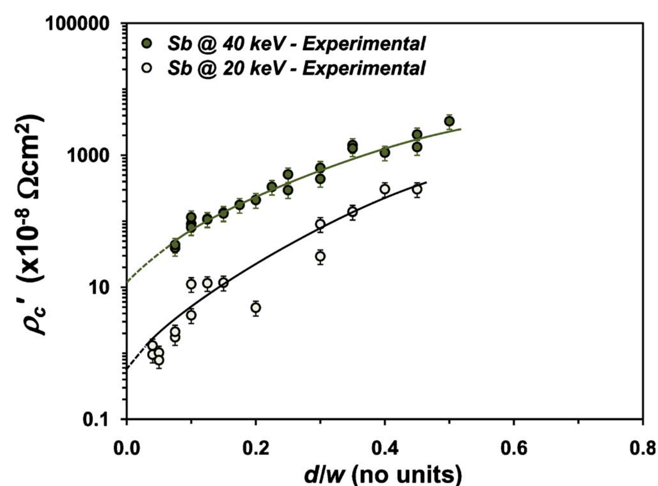

Figure 6. (Color online) Comparison of measured SCR values after 90 min of annealing at 300°C for CKR test structures with silicide arm width of 20 μm. These curves compare samples with antimony implanted at 20 and 40 keV. The lines of least-squares fit for each set of data points are shown, with the dotted lines used only to assist the reader in extrapolation of the data.

Table IV. Measured and estimated values of SCR for Al/NiSi/B-doped Si (implantation energy of 23.5 keV) ohmic contacts annealed at 300°C for different annealing durations (CKR arm width of 20 μm).

Anneal time (min)	$\rho'_{c(max)}$ (Ω cm^2)	$\rho'_{c(min)}$ (Ω cm^2)	ρ_c (Ω cm^2)
0	8.5×10^{-5}	2.1×10^{-7}	$1.0 \pm 0.5 \times 10^{-7}$
30	8.2×10^{-6}	2.9×10^{-8}	$9.0 \pm 1.0 \times 10^{-9}$
60	7.8×10^{-6}	1.2×10^{-8}	$3.5 \pm 0.5 \times 10^{-9}$
90	7.8×10^{-6}	1.0×10^{-8}	$3.5 \pm 0.5 \times 10^{-9}$

no difference. This evaluated value of 3.5×10^{-9} Ω cm^2 is the lowest reported value for a metal silicide contact to p-type doped silicon.

Figure 8 presents the measured SCR values obtained for CKRs with an arm width of 30 μm (after 90 min of annealing). This

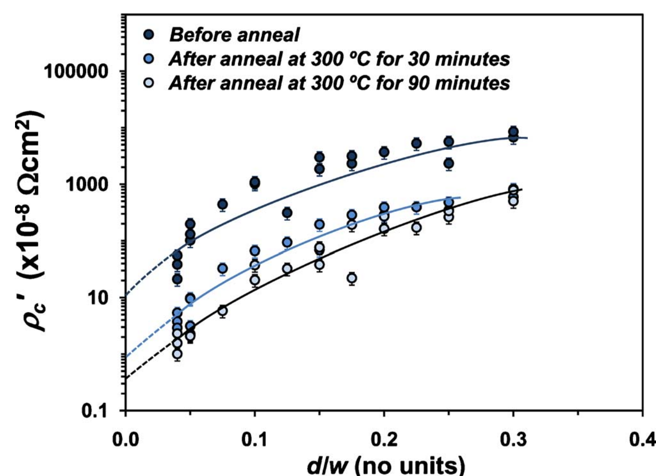

Figure 7. (Color online) Comparison of measured SCR values before and after various annealing steps at 300°C for CKR test structures with boron implantation and silicide arm width of 20 μm. These values were obtained by annealing the boron-implanted samples. The lines of least-squares fit for each set of data points are shown, with the dotted lines used only to assist the reader in extrapolation of the data.

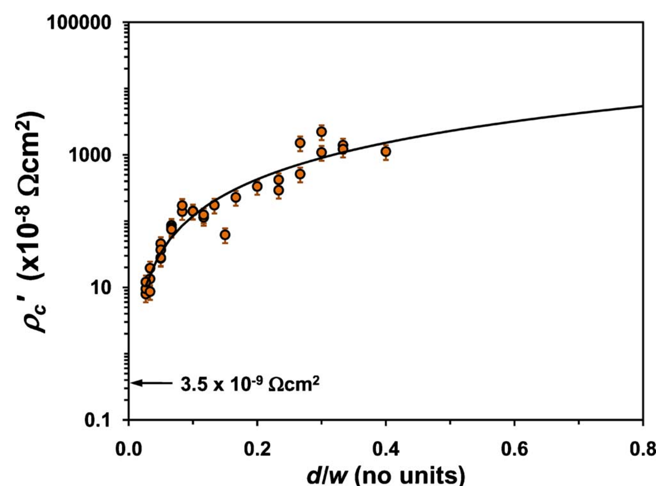

Figure 8. (Color online) Measured SCR values after 90 min of annealing at 300°C for CKR test structures with boron implantation and silicide arm width of 30 μm.

Downloaded on 2016-10-06 to IP 130.203.136.75 address. Redistribution subject to ECS terms of use (see ecsdl.org/site/terms_use) unless CC License in place (see abstract).

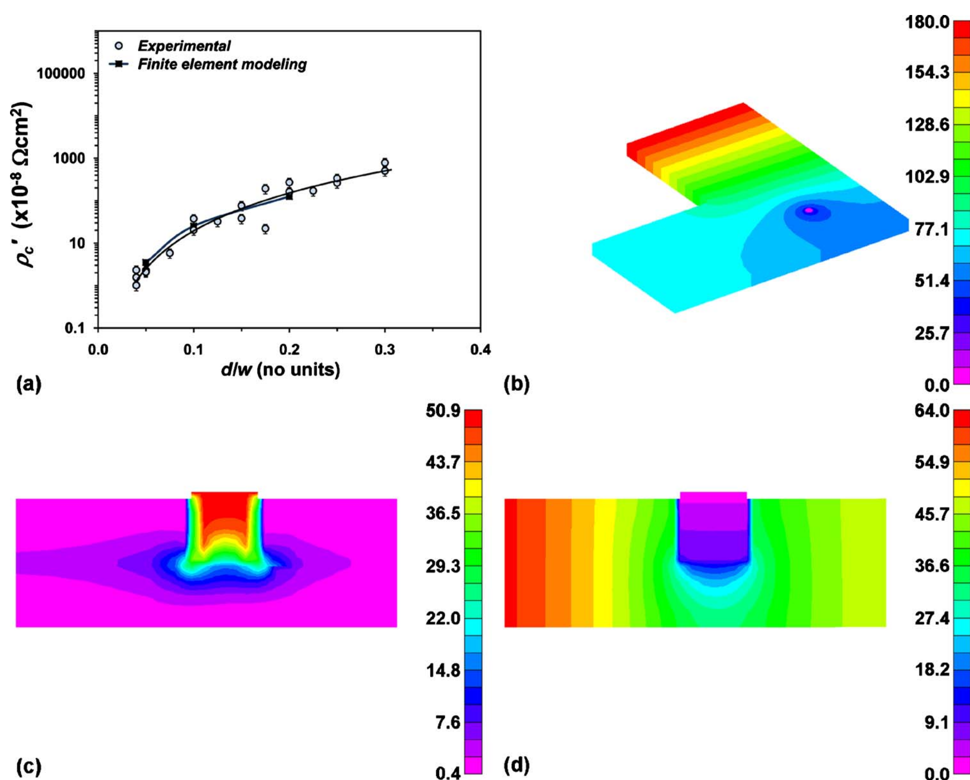

Figure 9. (Color online) (a) Comparison of measured SCR values for CKR test structures with boron implantation and silicide arm width of 20 μm with FEM results. (b) Voltage distribution in the three-dimensional model of the doped silicon "L." The (c) current density and (d) voltage drop as current flows through the doped silicon "L" and up the contact. All values shown on scale bars are in arbitrary units, with the modeling results in (b)-(d) corresponding to CKR with arm width w of 20 μm and contact diameter d of 1 μm ($d/w = 0.05$).

enables comparison between the results for the 20 and 30 μm CKR arm widths. These measured SCR values also extrapolate to a ρ_c of 3.5×10^{-9} Ω cm^2.

To bolster the experiment further, finite element modeling (FEM) was carried out with NASTRAN. Modeling was carried out for samples corresponding to those in Fig. 7: nickel silicide to boron-doped silicon and CKR test structures with an arm width of 20 μm. Three geometries were modeled for varying contact diameters (d = 1, 2, and 4 μm). The carrier concentration determined using SRIM in Table I and Ref. 18 was used to determine the resistivity of the doped region for these models. Assuming that the thickness of the doped region is the same as the ion range (considering a Gaussian distribution), the mean sheet resistance (R_{SH}) of the boron-doped region was determined to be 43.47 Ω/□. Figure 9a presents these FEM results and compares them with the experimental results presented previously in Fig. 7 for the curve related to the final result after annealing. Good agreement of these results is apparent, highlighting the veracity of the technique being applied to accurately determine such low values of SCR. The voltage and current distribution contours as shown by these models for the geometry corresponding to d/w of 0.05 is shown in the other three panels of this figure (Fig. 9b-d). For further accuracy, these models require the definition of an ion implanted layer of varying resistivity with depth, directly related to the Gaussian profile of the implant as shown by TRIM in Fig. 2c. Further refinements of these preliminary models related to ion implantation profiles is the scope for future work.

Conclusion

Low values of SCR for ohmic contacts incorporating nickel silicide have been evaluated. Measurements of SCR were carried out using CKR test structures for both antimony- and boron-doped samples. The influence of annealing on the SCR values is also reported. SCR values as low as 5.0×10^{-9} Ω cm^2 to antimony-doped (n-type) silicon and 3.5×10^{-9} Ω cm^2 to boron-doped (p-type) silicon were estimated. These values represent some of the lowest reported for a metal silicide contact to n-type silicon, whereas the value of 3.5×10^{-9} Ω cm^2 is the lowest value reported for a metal silicide contact to p-type doped silicon. Preliminary FEM results for Al/NiSi/B-doped Si ohmic contacts are also discussed, showing good agreement with experimental outcomes.

Acknowledgments

The authors acknowledge partial support for this project from the Australian Institute of Nuclear Science and Engineering and thank Dr. Peter J. Evans for his assistance. Authors Bhaskaran and Sriram contributed equally to this work.

RMIT University assisted in meeting the publication costs of this article.

References

1. International Technology Roadmap for Semiconductors (ITRS), 2006 update (available online at http://www.itrs.net/links/2006Update/FinalTo-Post/09_Interconnect2006Update.pdf).
2. M. L. Roukes, *Sci. Am.*, **285**, 48 (2001).
3. D. K. Schroder, *Semiconductor Material and Device Characterization*, 3rd ed., pp. 127–184, John Wiley & Sons, Hoboken, NJ (2006).
4. M. Finetti, S. Guerri, P. Negrini, A. Scorzoni, and I. Suni, *Thin Solid Films*, **130**, 37 (1985).
5. M. Finetti, A. Scorzoni, and G. Soncini, *IEEE Electron Device Lett.*, **5**, 524 (1984).
6. W. M. Loh, S. E. Swirhun, T. A. Schreyer, R. M. Swanson, and K. C. Saraswat, *IEEE Trans. Electron Devices*, **34**, 512 (1987).
7. A. Scorzoni and M. Finetti, *IEEE Trans. Electron Devices*, **35**, 386 (1988).
8. A. S. Holland, G. K. Reeves, and P. W. Leech, *IEEE Trans. Electron Devices*, **51**, 914 (2004).
9. M. Bhaskaran, S. Sriram, and A. S. Holland, *IEEE Electron Device Lett.*, **29**, 259 (2008).
10. N. Stavitski, M. J. H. van Dal, A. Lauwers, C. Vrancken, A. Y. Kovalgin, and R. A. M. Wolters, *IEEE Trans. Electron Devices*, **55**, 1170 (2008).
11. N. Stavitski, J. H. Klootwijk, H. W. van Zeijl, A. Y. Kovalgin, and R. A. M. Wolters, *IEEE Trans. Semicond. Manuf.*, **22**, 146 (2009).
12. A. S. Holland, G. K. Reeves, M. Bhaskaran, and S. Sriram, *IEEE Trans. Electron Devices*, **56**, 2250 (2009).
13. L. A. Clevenger and R. W. Mann, in *Properties of Metal Silicides*, K. Maex and M. van Rossum, Editors, INSPEC, London (1995).
14. M. Bhaskaran, S. Sriram, D. R. G. Mitchell, K. T. Short, A. S. Holland, and A. Mitchell, *Micron*, **40**, 11 (2009).
15. M. Bhaskaran, S. Sriram, A. S. Holland, and P. J. Evans, *Micron*, **40**, 99 (2009).
16. J. P. Biersack and L. G. Haggmark, *Nucl. Instrum. Methods*, **174**, 257 (1980).
17. J. F. Ziegler, *The Stopping and Range of Ions in Matter*, Vols. 2–6, Pergamon Press, Elmsford, NY (1985).
18. J. D. Plummer, M. D. Deal, and P. B. Griffin, *Silicon VLSI Technology: Fundamentals, Practice and Modeling*, p. 18, Prentice-Hall, Englewood Cliffs, NJ (2000).

Downloaded on 2016-10-06 to IP 130.203.136.75 address. Redistribution subject to ECS terms of use (see ecsdl.org/site/terms_use) unless CC License in place (see abstract).